Digital Predistortion of Single and Concurrent Dual-Band Radio Frequency GaN Amplifiers With Strong Nonlinear Memory Effects

Shoaib Amin, *Student Member, IEEE*, Peter Händel, *Senior Member, IEEE*, and Daniel Rönnow, *Member, IEEE*

***Abstract*— Electrical anomalies due to trapping effects in gallium nitride (GaN) power amplifiers (PAs) give rise to long-term or strong memory effects. We propose novel models based on infinite impulse response fixed pole expansion techniques for the behavioral modeling and digital predistortion of single-input single-output (SISO) and concurrent dual-band GaN PAs. Experimental results show that the proposed models outperform the corresponding finite impulse response (FIR) models by up to 17 dB for the same number of model parameters. For the linearization of a SISO GaN PA, the proposed models give adjacent channel power ratios (ACPRs) that are 7–17 dB lower than the FIR models. For the concurrent dual-band case, the proposed models give ACPRs that are 9–14 dB lower than the FIR models.**

***Index Terms*— Behavioral modeling, concurrent dual band, digital predistortion (DPD), finite impulse response (FIR), infinite impulse response (IIR), power amplifiers (PAs), radio frequency, single-input single-output (SISO).**

I. Introduction

GALLIUM nitride (GaN)-based power amplifiers (PAs) have the potential to be the long-term replacement for laterally diffused metal–oxide–semiconductor (LDMOS) technology in the future base station (BS) applications. LDMOS transistors have been employed as the technology of choice for high PAs in cellular BSs [1]. The advantages of LDMOS PAs are their high power, operating temperatures, and reliability levels [2]. However, because of new requirements in the future communication standards, e.g., 4G LTE and beyond, the LDMOS-based PAs may reach their limitations, i.e., in operational frequency and power efficiency.

GaN-based PAs have the advantage of higher operating temperatures, power efficiency, and higher breakdown voltages [3]–[5]. However, there are still challenges regarding electrical anomalies due to the trapping effects [6]–[8] that have time constants that are much larger than the period of a typical RF carrier signal [3], [4]. Compared with LDMOS-based PAs, where the memory effects are the same as or smaller than the period of the RF carrier signal, the linearization or digital predistortion (DPD) of GaN-based PAs is more difficult because of the presence of strong memory effects [4], [5], [9]. Hence, models for behavioral modeling or DPD of GaN PAs must include long-term memory effects.

DPD has been used extensively for linearization in the past decade [4], and it can also mitigate the PA's memory effects. DPD incorporates an inverse nonlinear dynamic transfer function of PA and is used for the linearization. This transfer function can be modeled using a Volterra series (VS) [10]. Due to the dimensionality issue of the VS, numerous algorithms based on memory polynomials have been proposed for the behavioral modeling and DPD of single-input single-output (SISO) PAs [11]–[14], all of which are subsets of the VS.

Concurrent dual-band PAs are used to increase the data rate and efficiency of wireless networks [15]–[18]. In concurrent dual-band PAs, the amplifier is excited with two signals operating at two different carrier frequencies, where the frequency spacing between the two carrier frequencies is of the order of hundreds of megahertzes to gigahertzes [19]. Moreover, the nonlinear behavior of concurrent dual-band PAs is different, i.e., the nonlinear function operates concurrently on both input signals, which results in cross-modulation (CM) distortion [19]. For the behavioral modeling and DPD of concurrent dual-band PAs, several algorithms have been proposed in the literature to model and compensate the nonlinear dynamic effects. In [20], a 2D-VS has been proposed, whereas in [21] and [22], a 2D memory polynomial (2D-MP) and a 2D generalized MP (GMP) model are proposed, respectively.

In recent years, the linearization of GaN-based SISO PAs has been reported in [23]–[25], where SISO GMP and MP models and their variants were used. Similarly, in [15], a 2D-MP model proposed in [21] was used to linearize a concurrent dual-band GaN PA, and in [17], the performance of a reduced 2D-VS is compared with the performance of the 2D-MP model for linearization of concurrent dual-band GaN PA and is reported to be the same.

However, these models and those in [11]–[14] and [20]–[22] for SISO and concurrent dual-band PAs, respectively, are based on finite impulse response (FIR) structures and, therefore, model memory effects of finite time. Hence, modeling of PAs that have time constants that are much larger than the sampling time requires the use of more parameters to capture memory effects, and overmodeling may be a problem. As reported

Manuscript received September 1, 2016; revised November 14, 2016 and December 12, 2016; accepted December 18, 2016. Date of publication February 14, 2017; date of current version June 29, 2017.

S. Amin is with the Department of Electronics, Mathematics and Natural Sciences, University of Gävle, SE-80176 Gävle, Sweden, and also with the Department of Signal Processing, ACCESS Linnaeus Centre, KTH Royal Institute of Technology, SE-10044 Stockholm, Sweden (e-mail: shoaib.amin@hig.se).

P. Händel is with the Department of Signal Processing, ACCESS Linnaeus Centre, KTH Royal Institute of Technology, SE-10044 Stockholm, Sweden (e-mail: ph@kth.se).

D. Rönnow is with the Department of Electronics, Mathematics and Natural Sciences University of Gävle, SE-80176 Gävle, Sweden (e-mail: daniel.ronnow@hig.se).

Color versions of one or more of the figures in this paper are available online at http://ieeexplore.ieee.org.

Digital Object Identifier 10.1109/TMTT.2016.2642948

in [3], burst signals may introduce long-term dynamic effects, such as bias circuit modulation, charge trapping, and self-heating in GaN PAs, and thus require behavioral and DPD models that incorporate such effects.

In [3] and [26], the average power in a long time window is added to the conventional SISO GMP and MP models when the PAs are excited with burst signals to address long-term memory effects. However, the total number of model parameters increases significantly [3], [26]. These models are based on FIR structures. In [27]–[29], SISO behavioral models that combine FIR and infinite impulse response (IIR) structures were proposed for modeling PAs with short-term and long-term memory effects.

In this paper, we have revisited the VS based on orthonormal bases functions [30]–[34] for SISO PAs. In these models, the input signals are filtered by IIR filters and then used in the VS. We use this approach to derive two novel behavioral/DPD models for SISO and three behavioral/DPD models for concurrent dual-band PAs that have memory effects with long time constants compared with the sampling time. The proposed models for SISO PAs are compared experimentally with FIR-based VS, MP [11], and GMP [35] models. Similarly, three novel models for concurrent dual-band PAs are compared with the models presented in [20] and [21]. The experimental results presented in this paper show that the proposed models outperform the corresponding FIR models when they are used for behavioral modeling and linearization of the SISO and concurrent dual-band GaN PAs. The proposed models could solve the challenging problem of linearizing GaN PAs with long-term memory effects [3].

This paper is organized as follows. In Section II, a previously published VS based on orthonormal-basis functions is revisited and novel models for SISO and concurrent dual-band amplifiers are proposed. Section III describes the experimental setup. Measurement results are presented and discussed in Section IV, and conclusions are drawn in Section V.

II. Modeling of SISO/MISO PAs With FP-Based Models

To address the issue of SISO nonlinear systems with long-term memory, VS based on orthonormal-basis functions and fixed pole expansion technique (hereafter, referred to as FP-VS) was proposed in [30]–[32], and later used as behavioral and DPD algorithms for SISO PAs in [34] and [36], respectively. The FP-VS retains the general properties of conventional FIR-VS [30], [34], i.e., any nonlinear dynamic system with fading memory can be modeled. In addition, the number of required parameters reduces drastically if properly designed orthonormal-basis functions are used [34], [37]. However, the FP-based models require nonlinear optimization techniques for the identification of the pole locations.

Most behavioral models for PAs are reduced forms of the FIR-VS, i.e., the set of basis functions is a subset of the set of basis functions of the FIR-VS. The reduced forms do not have the same general properties as the FIR-VS but they have manageable numbers of basis functions and can often be physically motivated. In the FP-VS, the input signal is filtered by IIR filters. The FIR-VS is a special case of the FP-VS with the poles of the IIR filters at the origin. *In this paper, we formulate FP models that are reduced forms of the FP-VS in the same way as the FIR-MP and FIR-GMP models are reduced forms of the FIR-VS.*

We briefly describe the SISO FP-VS [30], [34], and then propose two novel FP polynomial models for SISO PAs and three novel FP models for concurrent dual-band PAs. All models are odd-order complex baseband models, since the difference in performance between the odd and odd-even polynomials is negligible [38]. To the best of our knowledge, these models have not been previously proposed.

A. Fixed Pole Volterra Series

A discrete-time, odd-order FP-VS with input and output signals $u(n)$ and $y(n)$, respectively, can be described as [34]

$$y(n) = \sum_{\substack{p=1 \\ p:\text{odd}}}^{P} \sum_{m_1=0}^{N_1-1} \cdots \sum_{m_p=0}^{N_p-1} k_{p,m_1,\ldots,m_p} \cdot \prod_{d=1}^{\frac{p+1}{2}} v_{p,m_d}(n) \prod_{d=\frac{p+1}{2}+1}^{p} v^*_{p,m_d}(n) \tag{1}$$

where P is the maximum nonlinear order, N_1 is the number of basis functions for order 1, and $k_{p,m_1,\ldots,m_p}$ are the model parameters. The parameters are symmetric under all permutations of $m_1, \cdots, m_{p+1/2}$ and $m_{p+1/2+1}, \cdots, m_p$. In (1), $(\cdot)^*$ denotes the complex-conjugate operator, and $v_{p,m_d}(n)$ is a filtered version of $u(n)$ as the pth output of the IIR filter

$$G_{p,m+1}(z) = \sqrt{1-|\xi_{p,m}|^2}\frac{z}{z-\xi_m}\prod_{q=1}^{m}\frac{1-\xi^*_{p,q}}{z-\xi_{p,q}}, \quad m = 1, 2, \ldots, N \tag{2}$$

where $G_{p,m+1}(z)$ are orthonormal-basis functions [30], [39], and $\xi_{p,m}$ are the stable poles of $G_{p,m+1}(z)$, i.e., $(\xi_{p,m} \in \mathbb{C} : |\xi_{p,m}| < 1)$ [37]. The time domain realization $g_{p,m+1}(l)$ is given by the inverse Z transform of (2).

By setting all $\xi = 0$, (2) simplifies to $G_{p,m+1}(z) = z^{-(m-1)}$ and (1) becomes the FIR-VS. Moreover, by setting $\xi = 0$ and $N_1, \ldots, N_p = 1$, (1) becomes a static polynomial. We use only one pole per order and denote these $\xi^{(i,s)} = [\xi_1 \;\; \xi_3 \cdots \xi_p]$, where i denotes the output channel for concurrent dual-band models, and s denotes self-kernels. For cross kernels, we use c (explain later in text).

B. Fixed Pole Memory Polynomial

To reduce the number of parameters of the FP-VS in (1), we set $m_1 = m_2 = \cdots = m_p = m$, and $N_1 = \cdots = N_p = N$, and obtain the following:

$$y(n) = \sum_{\substack{p=1 \\ p:\text{odd}}}^{P} \sum_{m=0}^{N-1} k_{p,m} v_{p,m}(n)|v_{p,m}(n)|^{(p-1)}. \tag{3}$$

We refer to (3) as the FP-MP model for SISO PAs. In (3), $k_{p,m}$ are the model parameters, and $v_{p,m}(n)$ is the output of an IIR

filter, as in (2). Note that the FP-MP model only contains the main diagonal terms of FP-VS. The FP-MP model can hence model the long-term memory effects in a system with significantly reduced model parameters. By setting the pole at the origin, (3) becomes an FIR-MP model [4], [11].

C. Fixed Pole Generalized Memory Polynomial

To derive an FP-GMP model, we first consider the FP-VS and by setting $m_1 = m_a$, and introducing $l_{d-1} = m_d - m_a$ where $d = 2, 3 \ldots p$, (1) becomes

$$y(n) = \sum_{\substack{p=1 \\ p:\text{odd}}}^{P} \sum_{m_a=0}^{N_1-1} \sum_{l_1=0}^{N_2-1} \cdots \sum_{l_{p-1}=0}^{N_p-1} k_{p,m_a,l_1,\ldots,l_{p-1}} \cdot \upsilon_{p,m_a}(n) \prod_{d=2}^{\frac{p+1}{2}} \upsilon_{p,l_{d-1}+m_a}(n) \prod_{d=\frac{p+1}{2}+1}^{p} \upsilon^*_{p,l_{d-1}+m_a}(n) \tag{4}$$

by setting $l_1 = \cdots = l_{p-1} = m_b$, $N_1 = N_a$, and $N_2 = \cdots = N_p = N_b$, then (4) simplifies to

$$y(n) = \sum_{\substack{p=1 \\ p:\text{odd}}}^{P} \sum_{m_a=0}^{N_a-1} \sum_{m_b=0}^{N_b-1} k_{p,m_a,m_b} \cdot \upsilon_{p,m_a}(n) |\upsilon_{p,m_a+m_b}(n)|^{(p-1)} \tag{5}$$

where we refer to (5) as an FP-GMP model. In (5), k_{p,m_a,m_b} are the model parameters. υ_{p,m_a} and υ_{p,m_a+m_b} are the outputs of IIR filters as in (2). We use the same poles for υ_{p,m_a} and υ_{p,m_a+m_b} but different poles could also be used. The FP-GMP model is a subset of the FP-VS and the FP-MP model is a subset of the FP-GMP model. By setting the poles at the origin, (5) becomes the reduced FIR-GMP model [35], [40].

D. 2D Fixed Pole Volterra Series

The input–output relationship of a concurrent dual-band PA can be described as [20]

$$y(n) = f(u_1(n)e^{j\omega_{c_1}T_s} + u_2(n)e^{j\omega_{c_2}T_s}) \tag{6}$$

where $f(\cdot)$ denotes the nonlinear function, ω_{c_1} and ω_{c_2} are the two operating carrier frequencies, and T_s is the sampling interval of the baseband signals.

For baseband equivalent models, we only consider the frequency components located around the carrier frequencies of each band. The signal bandwidth is much smaller than any of the carrier frequencies. Hence, even-order terms are ignored, since they fall outside the band of interest, and thus, they can be filtered out [20]. The nonlinear function $f(\cdot)$ operates concurrently on both the input signals. Therefore, the output at a particular carrier frequency is a function of both self-kernels (that cause intermodulation (IM) distortion) and cross kernels (that cause CM distortion) [19]. In [20], a discrete-time 2D-FIR-VS is presented for the behavioral modeling and DPD of concurrent dual-band PAs.

In the following, we propose a discrete-time 2D fixed pole expansion technique-based VS (hereafter referred to as the 2D-FP-VS) for concurrent dual-band PAs with long-term memory effects. This model is derived from the 2D-FP-VS with the input signals $u_1(n)$ and $u_2(n)$ replaced by filtered signals. The 2D-FP-VS is given as

$$y^{(i)}(n) = \sum_{p=0}^{P} \sum_{m_1=0}^{N_1-1} \cdots \sum_{m_{2p+1}=0}^{N_{2p+1}-1} \sum_{p'=1}^{p+1} k^{(i)}_{(2p+1,m_1,\cdots,m_{2k+1},p')} \cdot \prod_{d=1}^{p'} \upsilon^{(i)}_{2p+1,m_d}(n) \prod_{d=p'+1}^{2p'-1} \upsilon^{(i),*}_{2p+1,m_d}(n) \cdot \prod_{d=2p'}^{p'+p} \upsilon^{(j)}_{2p+1,m_d}(n) \prod_{d=p'+p+1}^{2p+1} \upsilon^{(j),*}_{2p+1,m_d}(n), \quad \text{where } i, j = [1, 2] \text{ and } i \neq j, \tag{7}$$

where $y^{(i)}(n)$ is the model output of the ith channel, and $\upsilon^{(i)}_{2p+1,m_d}(n)$ and $\upsilon^{(j)}_{2p+1,m_d}(n)$ are the outputs of IIR filters, as in (2), excited by the input signals from the ith and jth channel $u^{(i)}(n)$ and $u^{(j)}(n)$, respectively. The IIR filters excited by $u^{(i)}(n)$ and $u^{(j)}(n)$ may have different poles per nonlinear order for each channel, because the matching network(s) of concurrent dual-band PAs are optimized for the different carrier frequencies. Furthermore, in [19], it was found that self- and cross-distortion products have different memory effects.

The self-kernels have the same symmetry properties as the SISO kernel, whereas the cross kernels have lower symmetry. The third-order cross kernels have no symmetry properties. The fifth-order cross kernels for $p' = 1$ are symmetric under permutations of m_2, m_3 and m_4, m_5. The cross kernel for $p' = 2$ is symmetric under permutations of m_2, m_4. Note that by setting the poles at the origin, (7) becomes the 2D-FIR-VS [20].

E. 2D Fixed Pole Memory Polynomial

To tackle the dimensionality issue of the 2D-FP-VS, we propose an odd-order 2D-FP-MP model, which is a subset of the 2D-FP-VS. By setting $m_1 = \cdots = m_{2p+1} = m$ and $N_1 = \cdots = N_{2p+1} = N$ in (7), the 2D-FP-VS model reduces to

$$y^{(i)}(n) = \sum_{\substack{p=0 \\ p:\text{even}}}^{P-1} \sum_{\substack{q=0 \\ q:\text{even}}}^{p} \sum_{m=0}^{N-1} k^{(i)}_{p,q,m} \cdot \upsilon^{(i)}_{p,m}(n) |\upsilon^{(i)}_{p,m}(n)|^{p-q} |\upsilon^{(j)}_{q,m}(n)|^{q}. \tag{8}$$

In (8), $k^{(i)}_{p,q,m}$ are the model parameters, and $\upsilon^{(i)}_{p,m}(n)$ and $\upsilon^{(j)}_{q,m}(n)$ are the outputs of the IIR filters, as in (2), exited by $u^{(i)}(n)$ and $u^{(j)}(n)$, respectively. Note that the 2D-FP-MP only contains the main diagonal terms of the 2D-FP-VS. The 2D-FP-MP model can hence model the long-term memory effects in concurrent dual-band systems with significantly reduced model parameters. If the poles are at the origin, the 2D-FP-MP becomes the 2D-FIR-MP model [21].

F. 2D Fixed Pole Generalized Memory Polynomial

To derive a 2D-FP-GMP model, let us consider (7), and by setting $m_1 = m_a$ with $N_1 = N_a$, and $m_2 = m_a + m_b$ and

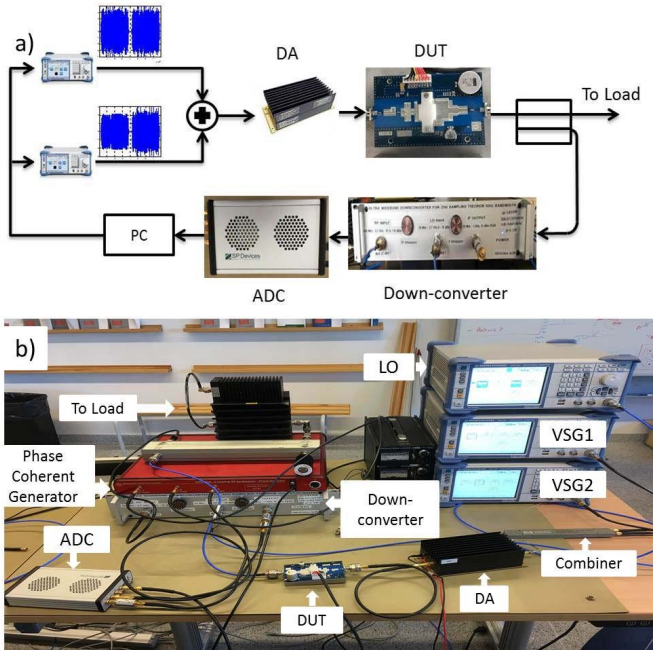

Fig. 1. (a) Outline of the measurement setup for concurrent dual-band measurements consisting of VSGs, DUT, downconverter, and an ADC. For SISO measurement, the same setup with single VSG was used. (b) Measurement setup used during experiments.

$m_3 = \cdots = m_{2p+1} = m_2$ with $N_2 = \cdots = N_{2p+1} = N_b$, the ith channel output of concurrent dual-band PAs can be modeled as

$$y^{(i)}(n) = \sum_{m_a=0}^{N_a-1} \sum_{\substack{p=0 \\ p:\text{even}}}^{P-1} \sum_{\substack{q=0 \\ q:\text{even}}}^{p} \sum_{m_b=0}^{N_b-1} k^{(i)}_{p,q,m_a,m_b} \cdot v^{(i)}_{p,m_a}(n)|v^{(i)}_{p,m_a+m_b}(n)|^{p-q}|v^{(j)}_{q,m_a+m_b}(n)|^{q} \quad (9)$$

where we refer to (9) as a 2D-FP-GMP model. The difference between (8) and (9) is the inclusion of some off-diagonal terms in addition to the main diagonal terms of (7). The 2D-FP-GMP model is a subset of the 2D-FP-VS and the 2D-FP-MP model is a subset of the 2D-FP-GMP model.

If all poles are at the origin, the 2D-FP-GMP model becomes

$$y^{(i)}(n) = \sum_{m_a=0}^{N_a-1} \sum_{\substack{p=0 \\ p:\text{even}}}^{P-1} \sum_{\substack{q=0 \\ q:\text{even}}}^{p} \sum_{m_b=0}^{N_b-1} h^{(i)}_{p,q,m_a,m_b} u^{(i)}(n-m_a) \cdot |u^{(i)}(n-m_a-m_b)|^{p-q}|u^{(j)}(n-m_a-m_b)|^{q} \quad (10)$$

where we refer to (10) as a 2D-FIR-GMP model. It is a subset of the model in [22]. The difference between the models in (10) and [22] is that (10) only contains lagging terms, whereas the model in [22] contains both leading and lagging terms. To the best of our knowledge, the model in (10) has not been proposed before.

III. Experimental Setup

A. Test Setup

The test setup shown in Fig. 1 consists of two Rohde & Schwarz SMBV100A vector signal generators (VSGs). The VSGs are baseband synchronized and use external local oscillators that are RF coherent. Baseband synchronization and RF coherency permit excellent control of the generated signals and low noise of the measured signals [19]. The VSGs have a maximum sampling rate of 150 MHz. The RF outputs of the VSGs were combined using a wideband combiner and its output was fed to the driver amplifier (DA) before the device under test (DUT), which is a GaN (Cree CGH21120F-AMP) PA. The RF output of the DUT was downconverted to intermediate frequency using a wideband downconverter and digitalized used an analog-to-digital converter (ADC). The ADC has a resolution of 14 b and a maximum sampling frequency of 400 MHz. Coherent averaging [41] is used to increase the dynamic range of the measurement system, and the spurious free dynamic range was 68 dB. For the SISO transmitter measurement, the same experimental setup was used except that only one of the two VSGs was used.

The DUT has an operating frequency band of 1.8–2.3 GHz with a single-carrier modulated gain of 15 dB. For the concurrent dual-band application, two carrier frequencies were used and generated with two VSGs, namely 1.9 and 2.2 GHz, respectively. For the SISO application, only one VSG was used and the carrier frequency was 1.9 GHz. The DA is a Mini-Circuits ZHL-42-W wideband amplifier with an operating frequency band of 10–4200 MHz, and a small signal gain of 34 dB (with ±1.3-dB gain flatness). The DA was operating in its linear region throughout the experiments.

B. DUT Characterization

In the following, we characterize the DUT with a two-tone [42], [43] and dual two-tone [19] test for SISO and concurrent dual-band scenarios, respectively. In a two-tone test, the asymmetry and frequency dependence of upper and lower third-order IM products *versus* frequency spacing is used as a qualitative measure of memory effects in the nonlinear transfer function of a device [42], [43]. For the SISO system, the frequency spacing between the tones was 20 kHz–10 MHz with a step size of 10 kHz. In the concurrent case, the frequency spacing for tones at 1.9 GHz was the same as for the SISO case, and for tones at 2.2 GHz, the frequency spacing was 15 kHz to 10.03 MHz.

Fig. 2(a)–(c) shows the measured amplitudes of the IM and CM products *versus* frequency spacing for the SISO and concurrent dual-band DUT, respectively. In Fig. 2(a) and (b), it can be observed that the amplitude of the IM products varies significantly *versus* frequency spacing, indicating the presence of nonlinear memory effects. Moreover, memory effects that contribute to asymmetry are also significant.

In order to characterize long- and short-term memory effects, the frequency spacing between the tones should be in order of few hertzes to kilohertzes and hundreds of kilohertzes to megahertzes, respectively [44]. From Fig. 2(a)–(c), it is observed that the slope of the IM and CM products *versus* frequency is negative at small and positive at large frequency spacing, which indicates different types of

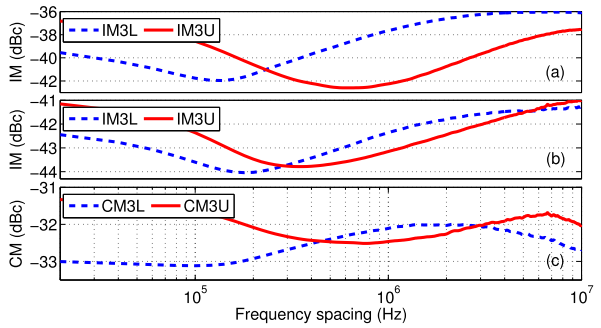

Fig. 2. (a) Measured amplitude of upper and lower third-order IM products *versus* frequency spacing for the SISO DUT. (b) and (c) Measured amplitude of upper and lower third-order IM and CM products *versus* frequency spacing for the concurrent dual-band DUT.

short- and long-term memory effects. It is common for RF PAs that the slope does not change sign with frequency (see [42]). The CM products exhibit small memory effects compared with the IM products, since the amplitude variation *versus* frequency is smaller. The asymmetry is large at small frequency spacing for IM and CM products, which indicates large-long-term memory effects.

Thus, the DUT introduces long- and short-term memory effects. The memory effects are larger for the IM products than for the CM products. The CM products are mostly affected by long-term memory effects, whereas the IM products are affected by both long- and short-term memory effects.

C. Excitation Signals

For the SISO measurements, three different carrier aggregated (CA) were used, where each CA signal was composed of two noncontiguous component carriers (CCs) operating at a carrier frequency of 1.9 GHz. The frequency spacing between the centers of the CCs was 50 MHz, i.e., CC_1 and CC_2 were at ∓ 25 MHz from the carrier frequency. The input signals have burst waveforms (with a burst on-period of 360 μs and an off-period of 40 μs), which may introduce dynamic effects, such as trapping charge phenomena, self-heating, and bias circuit modulation, that give rise to long-term memory effects [3].

In the first scenario, the DUT was excited by a CA signal, where the CCs consisted of two OFDM signals, each with a bandwidth of 10 MHz and peak-to-average-power-ratio (PAPR) of 11.42 dB. In the second scenario, the DUT was excited by a CA signal, where the CCs were composed of two four-carrier GSM signals, each with a bandwidth of 5 MHz and a PAPR of 8.89 dB. The last scenario was when the DUT was excited by a CA signal that combined an OFDM and a GSM signal with bandwidths of 10 and 5 MHz, respectively, and with a PAPR of 10.78 dB.

For concurrent dual-band measurements, the DUT was excited by two signals operating at the carrier frequencies of 1.9 and 2.2 GHz, respectively. Two scenarios were tested: 1) the DUT was excited by two OFDM signals, each with a bandwidth of 10 MHz and the PAPRs of 10.71 and 10.54 dB, respectively, and 2) the DUT was excited by an OFDM signal and a four-carrier GSM signal with bandwidths of 10 and 5 MHz, respectively, and PAPRs of 10.71 and 8.51 dB, respectively. For the identification and validation of model performance, separate signal sets were used.

D. System Identification

The output signal model of a concurrent dual-band PA can be written as

$$\begin{bmatrix} \mathbf{y}^i \\ \mathbf{y}^j \end{bmatrix} = \begin{bmatrix} \Psi^i(\xi^{(i)}, \mathbf{u}^{(i)}, \mathbf{u}^{(j)}) & 0 \\ 0 & \Psi^j(\xi^{(j)}, \mathbf{u}^{(j)}, \mathbf{u}^{(i)}) \end{bmatrix} \begin{bmatrix} \theta^i \\ \theta^j \end{bmatrix}, \quad i \neq j \tag{11}$$

where $\mathbf{y}^i$ is a column vector containing the measured output signal of the ith channel, θ_i is the vector of the unknown parameters, $\mathbf{u}^{(i)}$ and $\mathbf{u}^{(j)}$ are the vector of the input signals, and $\xi^{(i)}$ are the poles of the IIR filter in (2). $\Psi^i(\xi^{(i)}, \mathbf{u}^{(i)}, \mathbf{u}^{(j)})$ is the regression matrix, whose columns are the basis functions of the applied model. The basis functions are products of the signals $v^{(i)}_{p,m}$ and $v^{(j)}_{p,m}$, i.e., input signals $u^{(i)}(n)$ and $u^{(j)}(n)$ filtered by the IIR filters.

The parameters θ^i and ξ^i are identified by minimizing the cost function

$$S(\xi^{(i)}, \theta^i) = \arg\min_{\xi^{(i)}, \theta^i} \|y^i - \Psi^i(\xi^{(i)}, \mathbf{u}^{(i)}, \mathbf{u}^{(j)})\theta^i\|. \tag{12}$$

The models are linear in the parameter θ^i, and nonlinear in the poles $\xi^{(i)}$; thus, the identification is a separable least squares problem [45]. We used an iterative technique as in [29], [34], and [36] for the identification of pole location for RF PAs. Real valued poles were used. We tried different initial pole values but the identified optimal poles were the same. The poles were always found to be positive, i.e., the memory effects are of the low-pass character. Other identification methods that have been used for FP-VS, such as the Gauss–Newton [30] and backpropagation-through-time techniques [37], could also be used for our models. Note that for the DPD, the input and output signals are interchanged in (11) and (12). We use the indirect learning architecture [12], i.e., we identify the post-inverse of the system and use it as a pre-inverse.

E. Performance Evaluation

In order to evaluate the performance of given models, the metrics used are normalized mean-square error (NMSE), adjacent channel power ratio (ACPR), and adjacent channel error power ratio (ACEPR). NMSE and ACPR are defined by (13) and (14), respectively [46],

$$\text{NMSE} = \frac{\int \Phi_e(f)\, df}{\int \Phi_y(f)\, df}. \tag{13}$$

In (13), $\Phi_e(f)$ is the error signal's power spectrum and $\Phi_y(f)$ is the measured signal power spectrum

$$\text{ACPR} = \frac{\int_{\text{adj. ch.}} \Phi_y(f)\, df}{\int_{\text{ch.}} \Phi_y(f)\, df}. \tag{14}$$

The ACEPR is calculated as the ACPR, but with $\Phi_e(f)$ in the numerator.

TABLE I

PERFORMANCE EVALUATION OF GIVEN SISO BEHAVIORAL MODELS IN TERMS OF NMSE (dB) AND ACEPR (dB) WITH DIFFERENT EXCITATION SIGNALS. CC_1 AND CC_2 ARE AT THE OFFSET FREQUENCIES OF ∓ 25 MHz FROM THE CARRIER FREQUENCY

Models	OFDM-OFDM		GSM-GSM		OFDM-GSM	
	NMSE	ACEPR(CC_1/CC_2)	NMSE	ACEPR(CC_1/CC_2)	NMSE	ACEPR(CC_1/CC_2)
FIR-MP [4]	−36.4	−42.1/ − 41.9	−36.3	−43.2/ − 45.1	−37.0	−41.9/ − 44.4
FIR-GMP [35]	−38.9	−46.1/ − 42.5	−40.8	−48.5/ − 44.0	−40.9	−45.7/ − 48.0
FIR-VS	−41.3	−48.7/ − 50.1	−42.0	−50.4/ − 50.7	−41.6	−48.1/ − 49.8
FP-MP	−45.2	−55.2/ − 56.8	−46.7	−54.5/ − 56.3	−46.5	−54.9/ − 55.9
FP-GMP	−47.8	−57.3/ − 58.4	−51.0	−59.2/ − 59.3	−48.1	−56.1/ − 58.6
FP-VS [34]	−49.3	−59.8/ − 59.3	−53.3	−62.9/ − 63.1	−51.2	−58.9/ − 61.4

IV. RESULTS

In Section IV-A, we present the experimental results for the behavioral modeling and the DPD of the proposed models for SISO and concurrent dual-band PAs. The performance of the proposed models is compared with those of the corresponding FIR models. For the SISO DUT, the maximum nonlinear order (P) was 9. For the MP models, $N = 4$. For the GMP models, $N_a = 4$ and $N_b = 3$, and for the FP-VS and FIR-VS, $N_p = [4\,3\,2\,2\,2]$. With these choices of P and N, the SISO MP models have 25 model parameters, the GMP models have 65 model parameters, and the VS models have 570 model parameters.

For concurrent dual-band PA modeling and linearization, P was 9. For the 2D-MP models, $N = 5$; for the 2D-GMP models, $N_a = 4$ and $N_b = 3$, and for the 2D-VS, $N = [4\,3\,2\,1\,1]$. With these choices of P and N, the 2D-MP models have 90 model parameters per channel, the 2D-GMP models have 172 model parameters per channel, and the 2D-VS have 957 model parameters per channel.

These choices of P and N for the SISO and concurrent dual-band models resulted in the best model performance measured in terms of NMSE and ACEPR/ACPR. Further increases to P and N did not result in any reduction in the model error.

A. Behavioral Modeling—SISO PA

Table I summarizes the performance of proposed behavioral models for different excitation signals. The results for the corresponding FIR models are also shown. The FP models have NMSE values that are 7–11 dB lower than their corresponding FIR models. Similarly, the FP models have approximately 9–16 dB lower ACEPR values than their corresponding FIR models. The NMSE and ACEPR values are 0.5–5 dB lower for the GMP models than for the MP models (FIR and FP).

The performance variation between different test signals is small for the FP-MP model. However, for the FP-GMP and FP-VS models with OFDM signals, the models have NMSE values of −47.8 and −49.3 dB, respectively, which is 3–4 dB higher than the NMSE value obtained when the CCs were composed of GSM signals, and 3 dB higher for FP-VS when the CA signal was a combination of OFDM-GSM signals. Fig. 3 shows the model error spectrum for different behavioral models.

In Table I, it is observed that among the FP models, the FP-MP model resulted in the highest model error; however, it has 25 model parameters, i.e., approximately 23 times less parameters than the FP-VS. Moreover, the FP-GMP and FP-VS models resulted in approximately the same performance, where the FP-GMP model has 65 model parameters, i.e., approximately nine times less parameters than the FP-VS.

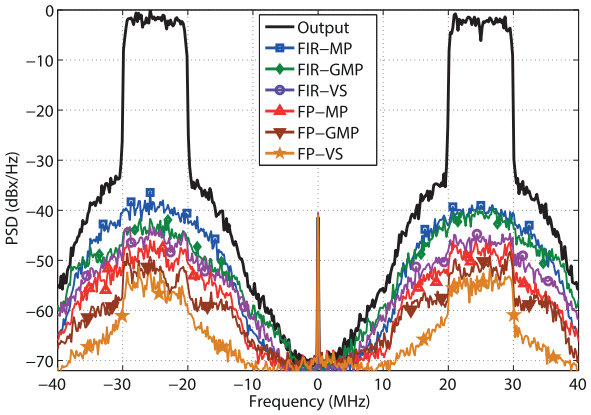

Fig. 3. Error spectrum of models for SISO GaN PA. The intraband noncontiguous CCs consists of two OFDM signals operating at an offset frequency of ± 25 MHz from the CF.

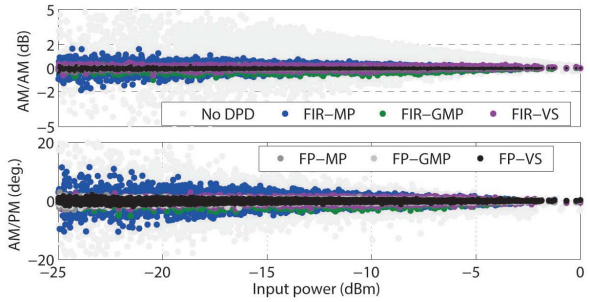

Fig. 4. (Top) AM/AM and (bottom) AM/PM of the SISO GaN PA. The compression at high input is concealed by the memory effects.

B. Linearization—SISO PA

Table II summarizes the performance of the given models when they are used as DPD algorithms under different excitations signals. The performance is measured in terms of NMSE, ACPR, and the total number of floating point operations (FLOPs). The amplitude-to-amplitude conversion (AM/AM) and amplitude-to-phase conversion (AM/PM) plots before and after linearization are shown in Fig. 4.

TABLE II

PERFORMANCE EVALUATION OF GIVEN SISO DPD MODELS IN TERMS OF NMSE (dB), ACPR (dB), AND TOTAL NUMBER OF FLOATING POINT OPERATIONS. CC_1 AND CC_2 ARE AT THE OFFSET FREQUENCIES OF ∓ 25 MHz FROM THE CARRIER FREQUENCY

Models	OFDM-OFDM		GSM-GSM		OFDM-GSM		FLOPs
	NMSE	ACPR(CC_1/CC_2)	NMSE	ACPR(CC_1/CC_2)	NMSE	ACPR(CC_1/CC_2)	
No DPD	−23.1	−34.3/ − 34.9	−24.0	−35.2/ − 35.4	−24.5	−34.7/ − 35.2	–
FIR-MP [4]	−36.6	−42.7/ − 42.2	−36.5	−44.0/ − 42.9	−37.5	−43.2/ − 48.5	209
FIR-GMP [35]	−38.9	−46.0/ − 44.6	−40.7	−49.1/ − 43.1	−41.7	−44.8/ − 49.4	529
FIR-VS	−40.6	−49.6/ − 51.7	−41.6	−48.2/ − 51.3	−42.0	−47.8/ − 51.9	7471
FP-MP	−44.9	−56.5/ − 56.6	−47.6	−55.6/ − 57.1	−46.0	−55.7/ − 56.2	230
FP-GMP	−47.6	−58.7/ − 59.5	−48.1	−58.6/ − 60.2	−47.9	−57.7/ − 60.7	550
FP-VS [34]	−48.2	−59.1/ − 60.1	−52.6	−61.5/ − 62.3	−51.5	−58.6/ − 61.3	7511

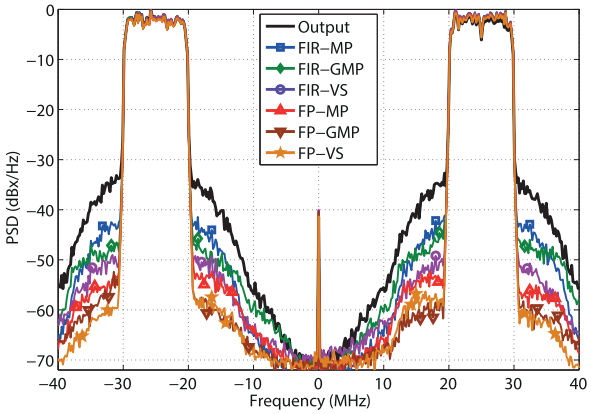

Fig. 5. Linearized output spectrum of the SISO DUT excited with noncontiguous CCs consisting of OFDM signals at an offset frequencies of ±25 MHz from the CF. The DPD algorithms are described in the legend.

Notice that large memory effects result in broadening of the AM/AM and AM/PM. Fig. 5 shows the linearized intraband noncontiguous output spectrum of CCs consisting of OFDM signals.

Under different test scenarios, DPD decreases the NMSE by a range of 12–13 dB for the FIR-MP, 15–17 dB for the FIR-GMP, and approximately 17 dB for the FIR-VS. In comparison, the FP-MP decreases the NMSE by a range of 21–24 dB, the FP-GMP decreases NMSE by 23–24 dB, and the FP-VS DPD decreases it by approximately 25–28 dB. Thus, the NMSE for the FP models is approximately 7–11 dB lower than the NMSE for the corresponding FIR models.

In terms of ACPR, for all the DPD test scenarios, the FP models resulted in ACPRs that are within −55.6 to −61.5 dB (−56.2 to −62.3 dB) for the offset frequencies that are −25(+25) MHz from the carrier frequency, which is well below the spectrum limit of −45 dB specified in [47] for intraband noncontiguous CCs. The FIR-MP resulted in an ACPR that is 1–3 dB above the maximum spectral emission limit for all test scenarios. Among the FIR models, only the FIR-VS resulted in an ACPR that is 3–7 dB lower than the maximum spectral emission limit [47]. However, it requires 7471 FLOPs. In comparison, the FP models result in ACPR values that are 7–17 dB lower than those of the FIR models and 10–17 dB below the spectrum limit. In terms of total number of FLOPs, the difference between the FP models and their corresponding FIR models is negligible. The FP-MP and GMP models require 230 and 550 FLOPs, respectively, which are 34.8 and 14.5 times lower than the FLOPs required by the FP-VS.

In comparison, the difference between the NMSE of the FIR/FP-MP and FIR/FP-GMP models is 0.5–4 dB. The corresponding ACPR values are 0.2–5 dB for FIR-MP and GMP models, and 2–4 dB for FP-MP and GMP models. The difference between NMSE of the GMP and VS (FP and FIR) models is 0.3–4 dB. The ACPR shows larger differences for the FIR models: for the FIR-MP, there is a 6-dB difference between the cases of the CCs consisting of OFDM signals and the case of OFDM-GSM signals (see CC_2 in Table II). Conversely, for the FP models, there are small variations in the ACPR values among the three test scenarios. Thus, the FP models are more robust than the FIR models with respect to changes of the signal type.

We have also used the setup [48] available online to compare the linearization performance of the FP-GMP with the corresponding FIR-GMP model. The setup [48] was excited with CCs composed of two OFDM signals operating at the offset frequencies, which are 50 MHz from the carrier frequency. The FP-GMP model resulted in the ACPR value of −53.3 (−49.9) dB for the offset frequency of +50 (−50) MHz, respectively, whereas the FIR-GMP model results in the ACPR value of −35.1 (−44.9) dB. The FP-GMP has an NMSE value of −43.7 dB, and this is 8.7 dB lower than the NMSE of the FIR-GMP model.

TABLE III

PERFORMANCE EVALUATION OF GIVEN MODELS IN TERMS OF NMSE (dB) AND ACEPR (dB) WHEN CONCURRENT DUAL-BAND PA WAS EXCITED WITH TWO 10-MHz-WIDE OFDM SIGNALS OPERATING AT THE CARRIER FREQUENCIES OF 1.9 AND 2.2 GHz, RESPECTIVELY

Models	Channel 1		Channel 2	
	NMSE	ACEPR	NMSE	ACEPR
2D-FIR-MP [21]	−38.9	−43.1	−38.8	−43.0
2D-FIR-GMP	−43.1	−48.3	−43.2	−46.5
2D-FIR-VS [20]	−44.8	−50.3	−44.3	−50.1
2D-FP-MP	−45.5	−52.9	−44.9	−51.8
2D-FP-GMP	−48.7	−55.3	−48.3	−55.1
2D-FP-VS	−49.3	−56.1	−49.0	−56.5

C. Behavioral Modeling—Concurrent Dual-Band PA

Table III summarizes the performance of the investigated models in terms of NMSE and ACEPR for the concurrent

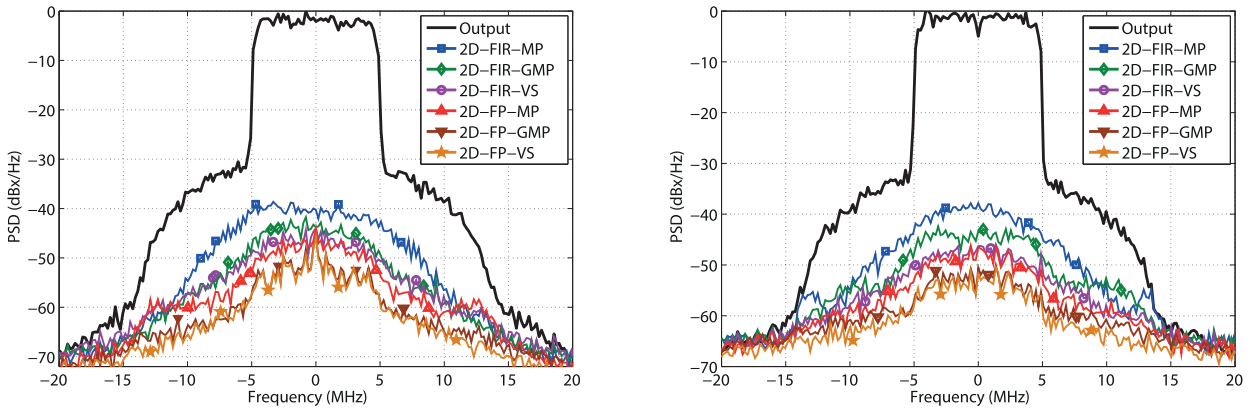

Fig. 6. Error spectrum for different behavioral models for channels 1 (left) and channel 2 (right) when the concurrent dual-band PA was excited with 10-MHz-wide OFDM signals operating at the carrier frequencies of 1.9 and 2.2 GHz.

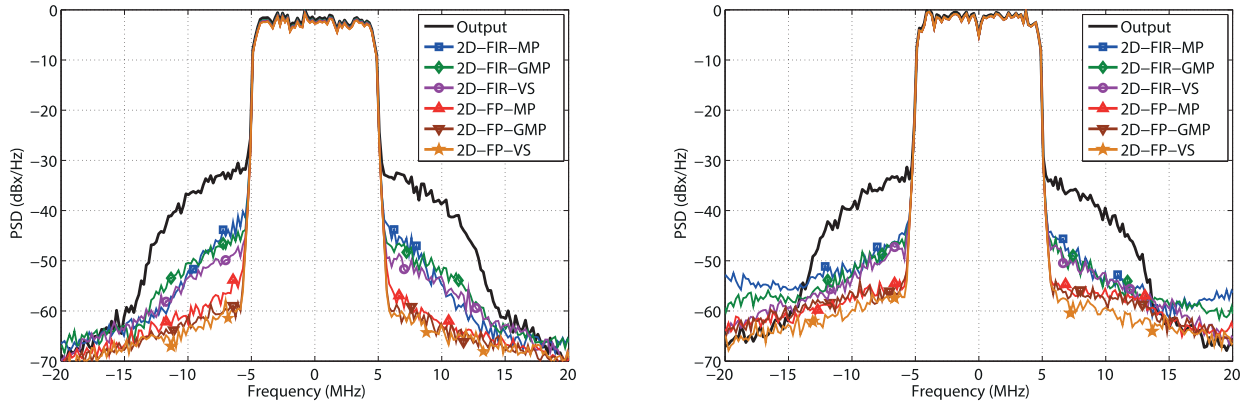

Fig. 7. Linearized output spectrum of channels 1 (left) and 2 (right) when the concurrent dual-band PA was excited with 10-MHz-wide OFDM signals operating at the carrier frequencies of 1.9 and 2.2 GHz.

dual-band PA excited with two OFDM signals operating at the carrier frequencies of 1.9 and 2.2 GHz, respectively. In Fig. 6, the measured output signal's power spectrum is given together with the error spectra of the different models. The FP models have NMSE values that are approximately 4–7 dB below those of the corresponding FIR models. For the ACEPR values, the results for FP models are 6–10 dB below those of the FIR models.

Among the FP models, the 2D-FP-MP model resulted in the highest model error and the 2D-FP-VS resulted in the lowest. The 2D-FP-GMP model resulted in model errors that are approximately the same (within 1 dB) as the 2D-FP-VS. The results for channels 1 and 2 are approximately the same.

Table IV summarizes the performance of the given models when the concurrent dual-band PA was excited with the OFDM and GSM signals operating at the carrier frequencies of 1.9 and 2.2 GHz, respectively. The FP models have NMSE and ACEPR values that are 2–5 and 4–8 dB lower than the corresponding FIR models. These differences are slightly smaller than those observed in the case of two OFDM signals (see Table III). The GSM signal has a smaller bandwidth than the OFDM signal and, hence, does not excite memory effects to the same extent. The results for channels 1 and 2 are approximately the same in Table IV. A comparison between Tables III and IV indicates that the 2D-FP-GMP and 2D-FP-VS models have the same performance for the two different signal cases. For the FIR-MP model, the NMSE in Table III is 2 dB higher than that in Table IV.

TABLE IV

PERFORMANCE EVALUATION OF GIVEN MODELS IN TERMS OF NMSE (dB) AND ACEPR (dB) WHEN CONCURRENT DUAL-BAND PA WAS EXCITED WITH A 10-MHz-WIDE OFDM AND A FOUR-CARRIER GSM SIGNAL OPERATING AT THE CARRIER FREQUENCIES OF 1.9 AND 2.2 GHz, RESPECTIVELY

Models	Channel 1		Channel 2	
	NMSE	ACEPR	NMSE	ACEPR
2D-FIR-MP [21]	−41.4	−46.8	−41.1	−45.0
2D-FIR-GMP	−45.7	−51.2	−44.9	−50.3
2D-FIR-VS [20]	−46.6	−52.8	−46.7	−51.7
2D-FP-MP	−46.3	−53.1	−46.5	−53.4
2D-FP-GMP	−48.7	−55.3	−48.8	−56.3
2D-FP-VS	−48.9	−56.8	−49.3	−57.1

D. Linearization—Concurrent Dual-Band PA

Fig. 7 shows the linearized output spectrum of channels 1 and 2 when the concurrent dual-band PA was excited with two OFDM signals. Table V summarizes the

TABLE V

PERFORMANCE EVALUATION OF GIVEN MODELS IN TERMS OF NMSE (dB) AND ACPR (dB) WHEN CONCURRENT DUAL-BAND PA WAS EXCITED WITH TWO 10-MHz-WIDE OFDM SIGNALS

Models	Channel 1		Channel 2	
	NMSE	ACPR	NMSE	ACPR
No-DPD	−23.6	−32.6	−23.1	−33.4
2D-FIR-MP [21]	−37.4	−42.2	−37.9	−45.6
2D-FIR-GMP	−40.7	−45.0	−40.5	−47.7
2D-FIR-VS [20]	−42.4	−49.8	−42.9	−48.2
2D-FP-MP	−44.1	−56.4	−44.4	−55.3
2D-FP-GMP	−48.5	−58.9	−47.0	−56.8
2D-FP-VS	−48.6	−59.6	−47.8	−58.0

TABLE VI

CONCURRENT DUAL-BAND MODEL COMPLEXITY IN TOTAL NUMBER OF FLOPS AND PARAMETERS PER CHANNEL

Models	FLOPs	Parameters
2D-FIR-MP [21]	752	90
2D-FIR-GMP	1408	172
2D-FIR-VS [20]	13363	957
2D-FP-MP	804	90
2D-FP-GMP	1460	172
2D-FP-VS	13519	957

performance of the proposed 2D-FP models in comparison with the 2D-FIR models when they are used as DPD algorithms and Table VI gives the model complexity with respect to the total number of FLOPs and model parameters per channel. In the following, we only summarize the results for two OFDM signals operating at the carrier frequencies of 1.9 and 2.2 GHz, respectively.

The results for channels 1 and 2 are approximately the same for all the applied models. Without DPD, the NMSE and ACPR values are approximately −23 and −33 dB, respectively. The lowest NMSE and ACPR values are obtained by using the 2D-FP-VS and they are −48 and −59 dB, respectively, for channel 1 and approximately −47 and −58 dB, respectively, for channel 2. The 2D-FP-GMP model gives approximately the same results as the 2D-FP-VS. Furthermore, the 2D-FP models give NMSE values that are 5–8 dB lower than those of the corresponding FIR models. Similarly, the ACPR is 9–14 dB lower for the 2D-FP models than the corresponding 2D-FIR models.

The GMP models give NMSE values that are 3–4 dB lower than the corresponding MP models for both 2D-FIR and 2D-FP models. The ACPR is 1–2 dB lower for the 2D-GMP models than the 2D-MP models (FP and FIR). Applying the 2D-FIR-VS as a DPD algorithm results in NMSE and ACPR values that are, respectively, 2 and 0.5–5 dB lower than those obtained when the 2D-FIR-GMP model is used. However, the 2D-FP-VS and 2D-FP-GMP models gives approximately the same NMSE and ACPR values.

If the same maximum spectral emission limit of −45 dB [47] is applied, the 2D-FIR-MP model does not meet the requirement in channel 1 and barely meets the requirement for channel 2, whereas the 2D-FIR-GMP marginally meets the maximum spectral emission limit. The 2D-FIR-VS is the only model among the 2D-FIR models

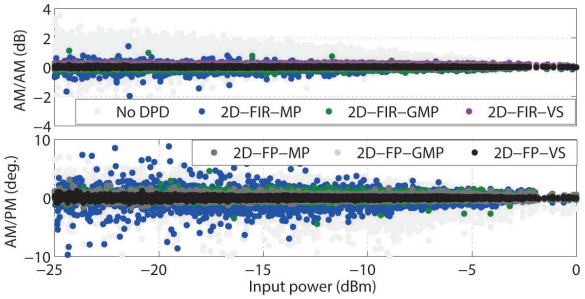

Fig. 8. (Top) AM/AM and (bottom) AM/PM of channel 1 of the concurrent dual-band GaN PA.

that satisfies the requirements in the adjacent channel with a margin of 3–5 dB. However, it requires 13 363 FLOPs. In contrast, the 2D-FP models results in ACPR values within a margin of approximately 10–15 dB from the spectrum limit. The analysis shows that the model complexity (see Table VI) of 2D-FP models can be reduced to meet the minimum required spectrum emission limit, which is not the case for the 2D-FIR models.

The improvement in NMSE/ACPR of the FP models compared with the FIR models is slightly smaller in the concurrent dual-band case (5–8/9–14 dB) than in the SISO case (7–11/7–17 dB). The lowest achieved NMSE/ACPR for the concurrent dual-band case (−48.6/ − 59.6 dB for the 2D-FP-VS) is approximately similar to the lowest achieved NMSE/ACPR for the SISO case (−48.2/ − 60.1 dB for FP-VS). Fig. 8 shows the AM/AM and AM/PM plots for channel 1 before and after linearization. For channel 2, the AM/AM and AM/PM looked practically the same.

E. Effect of Poles on Model Performance

In the following, a comparative analysis is presented on the performance of SISO and concurrent dual-band FP models with real and complex poles. Table VII summarizes the performance of SISO FP models when the DUT was excited with CCs consisting of two OFDM signals. The NMSE values for models with complex poles are 0.4–1.5 dB lower than those for models with real poles. The use of complex poles improves the model performance marginally and we conclude that real poles can be used for the GaN PA. The results were similar for the other types of signals.

SISO measurements showed that the identified poles for the DUT excited with CCs consisting of OFDM signals could be used for the DUT excited with CCs consisting of GSM and OFDM-GSM signals. When the poles given in Table VII are used for the DUT excited with OFDM-GSM signals, the FP-MP model results in an NMSE of −45.2 dB, which is 1.2 dB lower than the NMSE (see Table II) obtained using the optimum poles. Similarly, when poles given in Table VII are used for linearization of the DUT excited with CCs consisting of OFDM-GSM signals, the FP-GMP model results in an NMSE of −46.8 dB, which is 1.1 dB lower than the NMSE (see Table II) obtained from using the optimum poles. Similar observations were made for concurrent dual-band measurements when identified poles for the DUT excited

TABLE VII
POLE POSITIONS FOR FP-BASED MODELS WHEN THE SISO PA WAS EXCITED WITH A PAIR OF OFDM SIGNALS

Models	Poles					NMSE (dB)
	ξ_1	ξ_3	ξ_5	ξ_7	ξ_9	
FP-MP	0.0	0.3	0.5	0.5	0.5	−44.9
	$0.2\angle 149°$	$0.3\angle 343°$	$0.5\angle 343°$	$0.3\angle 332°$	$0.5\angle 11.4°$	−45.4
FP-GMP	0.0	0.3	0.6	0.6	0.6	−47.6
	$0.2\angle 149°$	$0.3\angle 355°$	$0.6\angle 360°$	$0.8\angle 355°$	$0.8\angle 355°$	−48.1
FP-VS	0.0	0.3	0.3	0.5	0.7	−48.2
	$0.2\angle 149°$	$0.2\angle 360°$	$0.3\angle 68.7°$	$0.5\angle 252°$	$0.7\angle 275°$	−49.7

with pair of OFDM signals were tested on the DUT excited with pair of OFDM and GSM signals. The 2D-FP-GMP model resulted in the NMSE values of −47.8 and −47.0 dB for channels 1 and 2, respectively, and the values are 1 dB higher than the NMSE values obtained with optimum poles.

F. Discussion

A physical interpretation of the used models is difficult due to the model and system complexity. Many behavioral models with FIR structure can be derived from a physically motivated block structure [4], which is a cascade of three subsystems. The first is a linear filter representing the PAs input matching network, the second is a static nonlinearity with a linear filter in a feedback circuit, and the third is a linear filter representing the output matching network. The FP models have parallel Wiener structures, i.e., linear filters followed by static nonlinearities. Physically, such models could be explained by input matching filter causing the memory effects. Such explanation is, however, not likely, since the linear terms have small memory effects.

In [49], a behavioral model for GaN amplifiers is presented. It contains one PA model for the short-term memory effects that correspond to the block structure in [4]. In addition, there is an outer feedback loop with a static nonlinearity and a linear filter, representing long-term memory effects. The proposed FP models have infinite memory and the poles should model both short- and long-term memory effects. The time of a burst (400 μs) is small compared with the time scale of seconds in [49], but large compared with time scales of FIR models (tens of nanoseconds). Furthermore, the FP models contain all products of all delayed terms, such as a Volterra model, but the respective parameters are not arbitrary but depend on the used poles. We, therefore, refrain from any further physical interpretation of the FP models.

V. CONCLUSION

Two novel models for SISO PA and three novel models for concurrent dual-band PA are presented for the behavioral modeling and DPD. In these models, the input signal(s) are filtered by the IIR filters that are FP expansions. The models, hence, have infinite memory depth. The performance of the proposed models is compared with that of corresponding FIR models for SISO and concurrent dual-band RF transmitters. The FP models for SISO PAs show a 7–11-dB improvement in their NMSE values compared with the corresponding FIR models when the models are used as DPD algorithms. Moreover, the complexity of the FP models is approximately the same as that of the FIR models in terms of FLOPs. In terms of ACPR values and with respect to the maximum spectral emission limit in the adjacent channels for intraband noncontiguous CCs, the proposed models give a margin of approximately 10–17 dB, whereas, for the FIR models, only the FIR-VS results in an ACPR with a margin of 3–7 dB with 7471 FLOPs.

A similar trend in the performance and complexity of 2D-FP models has been observed, where the 2D-FP models resulted in NMSE and ACPR values that are, respectively, 5–8 and −9–14 dB lower than their corresponding 2D-FIR models with approximately the same number of FLOPs. With respect to the minimum allowed spectral emission limits in the adjacent channels, the 2D-FP models give a margin of 10–15 dB when used as DPD algorithms, whereas the 2D-FIR models give a margin within 0–5 dB with the same level of complexity as the 2D-FP models measured in terms of FLOPs. We can conclude that the model complexity (in terms of FLOPs and number of parameters) of SISO and 2D-FP models can be reduced further to achieve the maximum spectral emission limit in the adjacent channels, whereas this is not the case for SISO and 2D-FIR models.

REFERENCES

[1] Y. Chung, J. Jeong, Y. Wang, D. Ahn, and T. Itoh, "Power level-dependent dual-operating mode LDMOS power amplifier for CDMA wireless base-station applications," *IEEE Trans. Microw. Theory Techn.*, vol. 53, no. 2, pp. 739–746, Feb. 2005.
[2] S. J. C. H. Theeuwen and J. H. Qureshi, "LDMOS technology for RF power amplifiers," *IEEE Trans. Microw. Theory Techn.*, vol. 60, no. 6, pp. 1755–1763, Jun. 2012.
[3] D. Lopez-Bueno, T. Wang, P. L. Gilabert, and G. Montoro, "Amping up, saving power: Digital predistortion linearization strategies for power amplifiers under wideband 4G5G burst-like waveform operation," *IEEE Microw. Mag.*, vol. 17, no. 1, pp. 79–87, Jan. 2016.
[4] J. Wood, *Behavioral Modeling and Linearization of RF Power Amplifiers*. Norwood, MA, USA: Artech House, 2014.
[5] O. Hammi and F. M. Ghannouchi, "Comparative study of recent advances in power amplification devices and circuits for wireless communication infrastructure," in *Proc. 16th IEEE Int. Conf. Electron. Circuits Syst.*, Dec. 2009, pp. 379–382.
[6] J. B. King and T. J. Brazil, "Nonlinear electrothermal GaN HEMT model applied to high-efficiency power amplifier design," *IEEE Trans. Microw. Theory Techn.*, vol. 61, no. 1, pp. 444–454, Jan. 2013.
[7] A. Jarndal, A. Z. Markos, and G. Kompa, "Improved modeling of GaN HEMTs on Si substrate for design of RF power amplifiers," *IEEE Trans. Microw. Theory Techn.*, vol. 59, no. 3, pp. 644–651, Mar. 2011.
[8] J. M. Tirado, J. L. Sanchez-Rojas, and J. I. Izpura, "Trapping effects in the transient response of AlGaN/GaN HEMT devices," *IEEE Trans. Electron Devices*, vol. 54, no. 3, pp. 410–417, Mar. 2007.
[9] B. Vassilakis and A. Cova, "Comparative analysis of GaAs/LDMOS/GaN high power transistors in a digital predistortion amplifier system," in *Proc. Microw. Conf., Asia–Pacific Conf. (APMC)*, vol. 2. Dec. 2005, pp. 1–4.
[10] S. Boyd and L. Chua, "Fading memory and the problem of approximating nonlinear operators with Volterra series," *IEEE Trans. Circuits Syst.*, vol. 32, no. 11, pp. 1150–1161, Nov. 1985.

[11] J. Kim and K. Konstantinou, "Digital predistortion of wideband signals based on power amplifier model with memory," *Electron. Lett.*, vol. 37, no. 23, pp. 1417–1418, Nov. 2001.

[12] D. R. Morgan, Z. Ma, J. Kim, M. G. Zierdt, and J. Pastalan, "A generalized memory polynomial model for digital predistortion of RF power amplifiers," *IEEE Trans. Signal Process.*, vol. 54, no. 10, pp. 3852–3860, Oct. 2006.

[13] S. Afsardoost, T. Eriksson, and C. Fager, "Digital predistortion using a vector-switched model," *IEEE Trans. Microw. Theory Techn.*, vol. 60, no. 4, pp. 1166–1174, Apr. 2012.

[14] Y.-J. Liu, J. Zhou, W. Chen, and B.-H. Zhou, "A robust augmented complexity-reduced generalized memory polynomial for wideband RF power amplifiers," *IEEE Trans. Ind. Electron.*, vol. 61, no. 5, pp. 2389–2401, May 2014.

[15] P. Saad *et al.*, "Concurrent dual-band GaN-HEMT power amplifier at 1.8 GHz and 2.4 GHz," in *Proc. IEEE 13th Annu. Wireless Microw. Technol. Conf.*, Apr. 2012, pp. 1–5.

[16] J. Pang, S. He, C. Huang, Z. Dai, C. Li, and J. Peng, "A novel design of concurrent dual-band high efficiency power amplifiers with harmonic control circuits," *IEEE Microw. Wireless Compon. Lett.*, vol. 26, no. 2, pp. 137–139, Feb. 2016.

[17] B. Fehri and S. Boumaiza, "Baseband equivalent Volterra series for digital predistortion of dual-band power amplifiers," *IEEE Trans. Microw. Theory Techn.*, vol. 62, no. 3, pp. 700–714, Mar. 2014.

[18] F. Mkadem, A. Islam, and S. Boumaiza, "Multi-band complexity-reduced generalized-memory-polynomial power-amplifier digital predistortion," *IEEE Trans. Microw. Theory Techn.*, vol. 64, no. 6, pp. 1763–1774, Jun. 2016.

[19] S. Amin, W. Van Moer, P. Händel, and D. Rönnow, "Characterization of concurrent dual-band power amplifiers using a dual two-tone excitation signal," *IEEE Trans. Instrum. Meas.*, vol. 64, no. 10, pp. 2781–2791, Oct. 2015.

[20] H. Qian, S. Yao, H. Huang, X. Yang, and W. Feng, "Low complexity coefficient estimation for concurrent dual-band digital predistortion," *IEEE Trans. Microw. Theory Techn.*, vol. 63, no. 10, pp. 3153–3163, Oct. 2015.

[21] S. A. Bassam, M. Helaoui, and F. M. Ghannouchi, "2D digital predistortion (2D-DPD) architecture for concurrent dual-band transmitters," *IEEE Trans. Microw. Theory Techn.*, vol. 59, no. 10, pp. 2547–2553, Oct. 2011.

[22] H. Cao, H. M. Nemati, A. S. Tehrani, T. Eriksson, and C. Fager, "Digital predistortion for high efficiency power amplifier architectures using a dual-input modeling approach," *IEEE Trans. Microw. Theory Techn.*, vol. 60, no. 2, pp. 361–369, Feb. 2012.

[23] M. V. D. Nair, R. Giofre, P. Colantonio, and F. Giannini, "Effects of digital predistortion and crest factor reduction techniques on efficiency and linearity trade-off in class AB GaN-PA," in *Proc. Eur. Microw. Conf.*, Sep. 2015, pp. 1128–1131.

[24] O. Hammi, M. S. Sharawi, and F. M. Ghannouchi, "Generalized twin-nonlinear two-box digital predistorter for GaN based LTE Doherty power amplifiers with strong memory effects," in *Proc. IEEE Int. Wireless Symp.*, Apr. 2013, pp. 1–4.

[25] T. Ota, H. Ishikawa, and K. Nagatani, "A novel adaptive digital predistortion for wideband power amplifiers with memory effects," in *Proc. Asia–Pacific Microw. Conf. (APMC)*, vol. 1. Dec. 2015, pp. 1–3.

[26] A. S. Tehrani, T. Eriksson, and C. Fager, "Modeling of long term memory effects in RF power amplifiers with dynamic parameters," in *IEEE MTT-S Int. Microw. Symp. Dig.*, Jun. 2012, pp. 1–3.

[27] M. Masood, C. Rey, S. Kenney, G. Norris, and R. Sherman, "RF power amplifier modeling for three-port applications using polynomials with IIR bases functions," in *Proc. IEEE Radio Wireless Symp.*, Jan. 2010, pp. 256–259.

[28] M. Masood, J. Wood, J. Staudinger, and J. S. Kenney, "Behavioral modeling of high power RF amplifiers using pruned Volterra scheme with IIR basis functions," in *Proc. IEEE Topical Conf. Power Modelling Wireless Radio Appl.*, Jan. 2012, pp. 97–100.

[29] A. S. Tehrani, H. Cao, T. Eriksson, and C. Fager, "Orthonormal-basis power amplifier model reduction," in *Proc. Workshop Integr. Nonlinear Microw. Millim.-Wave Circuits*, Nov. 2008, pp. 39–42.

[30] R. Hacioglu and G. A. Williamson, "Reduced complexity Volterra models for nonlinear system identification," *EURASIP J. Adv. Signal Process.*, vol. 2001, no. 4, pp. 257–265, 2001.

[31] R. J. G. B. Campello, W. C. Amaral, and G. Favier, "Optimal Laguerre series expansion of discrete Volterra models," in *Proc. Eur. Control Conf.*, Sep. 2001, pp. 372–377.

[32] R. J. Campello, G. Favier, and W. C. do Amaral, "Optimal expansions of discrete-time Volterra models using Laguerre functions," *Automatica*, vol. 40, no. 5, pp. 815–822, 2004.

[33] A. Zhu and T. J. Brazil, "RF power amplifier behavioral modeling using Volterra expansion with Laguerre functions," in *IEEE MTT-S Int. Microw. Symp. Dig.*, Jun. 2005, pp. 1–4.

[34] M. Isaksson and D. Rönnow, "A parameter-reduced Volterra model for dynamic RF power amplifier modeling based on orthonormal basis functions," *Int. J. RF Microw. Comput. Aided Eng.*, vol. 17, no. 6, pp. 542–551, 2007.

[35] T. R. Cunha, E. G. Lima, and J. C. Pedro, "Validation and physical interpretation of the power-amplifier polar Volterra model," *IEEE Trans. Microw. Theory Techn.*, vol. 58, no. 12, pp. 4012–4021, Dec. 2010.

[36] D. Ronnow and M. Isaksson, "Digital predistortion of radio frequency power amplifiers using Kautz–Volterra model," *Electron. Lett.*, vol. 42, no. 13, pp. 780–782, Jun. 2006.

[37] A. da Rosa, R. J. G. B. Campello, and W. C. Amaral, "Exact search directions for optimization of linear and nonlinear models based on generalized orthonormal functions," *IEEE Trans. Autom. Control*, vol. 54, no. 12, pp. 2757–2772, Dec. 2009.

[38] P. N. Landin and D. Rönnow, "RF PA modeling considering odd-even and odd order polynomials," in *Proc. IEEE Symp. Commun. Veh. Technol.*, Nov. 2015, pp. 1–6.

[39] B. Ninness and F. Gustafsson, "A unifying construction of orthonormal bases for system identification," *IEEE Trans. Autom. Control*, vol. 42, no. 4, pp. 515–521, Apr. 1997.

[40] M. Herman, B. Miller, and J. Goodman, "The cube coefficient subspace architecture for nonlinear digital predistortion," in *Proc. 42nd Asilomar Conf. Signals Syst. Comput.*, Oct. 2008, pp. 1857–1861.

[41] *IEEE Standard for Terminology and Test Methods of Digital-to-Analog Converter Devices*, IEEE Standard 1658-2011, Feb. 2012.

[42] D. H. Wisell, B. Rudlund, and D. Ronnow, "Characterization of memory effects in power amplifiers using digital two-tone measurements," *IEEE Trans. Instrum. Meas.*, vol. 56, no. 6, pp. 2757–2766, Dec. 2007.

[43] K. A. Remley, D. F. Williams, D. M. M.-P. Schreurs, and J. Wood, "Simplifying and interpreting two-tone measurements," *IEEE Trans. Microw. Theory Techn.*, vol. 52, no. 11, pp. 2576–2584, Nov. 2004.

[44] S. Boumaiza and F. M. Ghannouchi, "Thermal memory effects modeling and compensation in RF power amplifiers and predistortion linearizers," *IEEE Trans. Microw. Theory Techn.*, vol. 51, no. 12, pp. 2427–2433, Dec. 2003.

[45] G. H. Golub and V. Pereyra, "The differentiation of pseudo-inverses and nonlinear least squares problems whose variables separate," *SIAM J. Numer. Anal.*, vol. 10, no. 2, pp. 413–432, Feb. 1973.

[46] P. Landin, M. Isaksson, and P. Handel, "Comparison of evaluation criteria for power amplifier behavioral modeling," in *IEEE MTT-S Int. Microw. Symp. Dig.*, Jun. 2008, pp. 1441–1444.

[47] *ETSI TS 136 104—V12.5.0—LTE; Evolved Universal Terrestrial Radio Access (E-UTRA); Base Station (BS) Radio Transmission and Reception Version 12.5.0 Release 12*, Doc. TS 36.104, 3GPP, 2014.

[48] P. N. Landin, S. Gustafsson, C. Fager, and T. Eriksson, "WebLab: A Web-based setup for PA digital predistortion and characterization [application notes]," *IEEE Microw. Mag.*, vol. 16, no. 1, pp. 138–140, Feb. 2015.

[49] J. C. Pedro, P. M. Cabral, T. R. Cunha, and P. M. Lavrador, "A multiple time-scale power amplifier behavioral model for linearity and efficiency calculations," *IEEE Trans. Microw. Theory Techn.*, vol. 61, no. 1, pp. 606–615, Jan. 2013.

Shoaib Amin (S'12) received the B.E. degree in avionics engineering from the College of Aeronautical Engineering, National University of Sciences and Technology, Islamabad, Pakistan, in 2008, the M.Sc. degree in electronics from the University of Gävle, Gävle, Sweden, in 2011, the Licentiate degree in electrical engineering from the School of Electrical Engineering, KTH Royal Institute of Technology, Stockholm, Sweden, in 2015, and is currently pursuing the Ph.D. degree at the University of Gävle and the KTH Royal Institute of Technology.

His current research interests include signal processing techniques for characterization and mitigation of nonlinear dynamic effects in multiband multichannel RF transmitters.

Peter Händel (S'88–M'94–SM'98) received the M.Sc. degree in engineering physics and Lic.Eng. and Ph.D. degrees in automatic control from the Department of Technology, Uppsala University, Uppsala, Sweden, in 1987, 1991, and 1993, respectively.

From 1987 to 1988, he was a Research Assistant with The Svedberg Laboratory, Uppsala University. Between 1988 and 1993, he was a Teaching and Research Assistant with the Systems and Control Group, Uppsala University. From 1993 to 1997, he was with the Research and Development Division, Ericsson Radio Systems AB, Kista, Sweden. In 1996, he was a Docent with Uppsala University. Between 1996 and 1997, he was a Visiting Scholar with the Signal Processing Laboratory, Tampere University of Technology, Tampere, Finland, where he was a Docent in 1998. Since 1997, he has been with the School of Electrical Engineering, KTH Royal Institute of Technology, Stockholm, Sweden, where he is currently a Professor of Signal Processing and the Head of the Department of Signal Processing. He has held a part-time position as an Associate Director of Research, the Swedish Defense Research Agency, from 2000 to 2006. He has been a Guest Professor with the Indian Institute of Science, Bangalore, India, since 2010, spending some months in Bangalore. He was a Guest Professor with the University of Gävle between 2007 and 2013. He has conducted research in a wide area, including design and analysis of digital and adaptive filters, measurement and estimation theory, system identification, and speech processing. His current research interests include radio frequency measurement technology, indoor positioning and navigation, insurance telematics, and industrial digitalization.

Dr. Handel is a Registered Engineer (EUR ING). He is a former President of the IEEE Finland joint Signal Processing and Circuits and Systems Chapter and also the IEEE Sweden Signal Processing Chapter.

Daniel Rönnow (M'05) received the M.Sc. degree in engineering physics and Ph.D. degree in solid-state physics from Uppsala University, Uppsala, Sweden, in 1991 and 1996, respectively.

He was involved with semiconductor physics with the Max-Planck-Institut für Festkörperforschung, Stuttgart, Germany, from 1996 to 1998, and with infrared sensors and systems with Acreo AB, Stockholm, Sweden, from 1998 to 2000. From 2000 to 2004, he was a Technical Consultant and the Head of Research with Racomna AB, Uppsala, Sweden, where he was involved with PA linearization and with smart materials for microwave applications. From 2004 to 2006, he was a University Lecturer with the University of Gävle, Gävle, Sweden. From 2006 to 2011, he was a Senior Sensor Engineer with Westerngeco, Oslo Norway, where he was involved with signal processing and seismic sensors. In 2011, he became a Professor of electronics with the University of Gävle. He has been an Associate Professor with Uppsala University since 2000. He has authored or co-authored over 45 peer-reviewed papers and holds 8 patents. His current research interests include RF measurement techniques and linearization of nonlinear RF circuits and systems.